

Boosting Point-supervised Temporal Action Localization via Text Refinement and Alignment

Yunchuan Ma^{a,*}, Laiyun Qing^a, Guorong Li^a, Yuqing Liu^a, Yuankai Qi^b, Qingming Huang^a

^a*University of Chinese Academy of Science, Beijing, 100190, China*

^b*Macquarie University*

Abstract

Recently, point-supervised temporal action localization has gained significant attention for its effective balance between labeling costs and localization accuracy. However, current methods only consider features from visual inputs, neglecting helpful semantic information from the text side. To address this issue, we propose a Text Refinement and Alignment (TRA) framework that effectively utilizes textual features from visual descriptions to complement the visual features as they are semantically rich. This is achieved by designing two new modules for the original point-supervised framework: a Point-based Text Refinement module (PTR) and a Point-based Multimodal Alignment module (PMA). Specifically, we first generate descriptions for video frames using a pre-trained multimodal model. Next, PTR refines the initial descriptions by leveraging point annotations together with multiple pre-trained models. PMA then projects all features into a unified semantic space and leverages a point-level multimodal feature contrastive learning to reduce the gap between visual and linguistic modalities. Last, the enhanced multi-modal features are fed into the action detector for precise localization. Extensive experimental results on five widely used benchmarks demonstrate the favorable performance of our proposed framework compared to several state-of-the-art methods. Moreover, our computational overhead analysis shows that the framework can run on a single 24 GB RTX 3090 GPU, indicating its practicality and scalability.

Keywords: Point-Supervised Temporal Action Localization, Vision and Language,

^{*}Corresponding author

Email address: mayunchuan23@mails.ucas.ac.cn (Yunchuan Ma)

1. Introduction

Temporal Action Localization aims to localize and classify action instances in a long untrimmed video, which plays an essential role in various applications, such as highlight detection [1], security monitoring [2], and action spotting [3]. Traditional fully-supervised methods [4, 5, 6, 7, 8] have achieved high performance but require high-quality temporal boundary annotations, which are time-consuming and rarely readily available. In contrast, weakly-supervised temporal action localization (WTAL) [9, 10, 11, 12, 13], only requires video-level annotations (*i.e.*, only label which action categories are contained in a video). However, the lack of instance-level annotations in WTAL makes it challenging for models to distinguish actions from backgrounds, leading to inferior performance compared to fully-supervised methods.

To balance annotation labor cost and detection performance, point-supervised temporal action localization (PTAL) [14] is proposed, requiring only one single frame label for each action instance. As the pioneer, SF-Net [14] iteratively mines pseudo action frames and background frames to provide supplementary supervision during training. Following this setting, many researchers further propose various optimization methods. For example, LACP [15] designs a greedy algorithm to generate the dense optimal sequence and learns the completeness of the action instances from point annotations. TSPNet [16] leverages the prior knowledge that humans tend to annotate at the center of instances, and learns a center score to mitigate the misalignment issue. To alleviate the semantic ambiguity in determining action boundaries, Liu *et al.* [17] proposes a stepwise multi-grained boundary detector to locate the action boundaries. Meanwhile, Zhang *et al.* [18] proposes a two-stage learning framework, which learns the discriminative snippet-level scores to generate more reliable proposals and adjusts these proposals through instance-level feature learning.

Despite progress, existing methods [15, 18] only consider visual information, neglecting textual semantic features that could further enhance detection accuracy. To fully exploit high-level semantics, incorporating relevant textual information is favor-

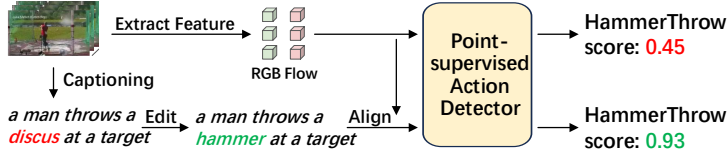


Figure 1: Previous approaches (upper branch) directly use visual features as the input to the detector, whereas our method (lower branch) first generates visual descriptions, then edits them for improved accuracy, and finally aligns multiple modalities as input to the detector.

able. Toward this goal, we propose a novel framework called Text Refinement and Alignment (TRA). Our work effectively improves the action localization precision by first integrating precisely refined textual descriptions, and then aligning the relevant visual and linguistic modalities. As shown in the lower part of Figure 1, unlike previous methods, we plug external visual descriptions as input and obtain more accurate class activation scores. Specifically, we begin by following traditional methods to segment the videos into dense short snippets, and then utilize an off-the-shelf caption generator (*i.e.*, BLIP2) to produce detailed captions for these snippets. Although powerful pre-trained captioning models can generate fluent captions, they might generate incorrect captions for different but similar actions (*e.g.*, throw a discus and throw a hammer). To alleviate the issue, we propose a Point-based Text Refinement (PTR) module to edit and enhance these sentences. Specific details of this module are provided later in Sec. 3.1. Subsequently, we extract features from different modalities and feed them into our proposed Point-based Multimodal Alignment (PMA) module for aligning. In PMA, we design a point-based multimodal contrastive learning loss to minimize the gap between different modalities of the same action as much as possible and increase the disparity between different action classes.

In summary, the main contributions of this paper are as follows:

- We identify the neglect of textual semantics in point-supervised temporal action localization and address it by leveraging point annotations to mine accurate textual semantics and fully exploit their potential.
- We propose a Text Refinement and Alignment (TRA) framework, which effectively refines general captions and aligns vision and language modalities, enhancing semantic information to improve localization precision.

- We design two new modules: the Point-based Text Refinement (PTR) module and the Point-based Multimodal Alignment (PMA) module. The former edits incorrect captions into correct ones with point annotations. The latter aligns visual and text modalities using predicted pseudo-point labels.
- Extensive experiments on the THUMOS’14, GTEA, BEOID, ActivityNet1.2, and ActivityNet1.3 datasets demonstrate the favorable performance of the proposed method compared to several state-of-the-art approaches. Furthermore, the computational overhead of our framework is moderate, and it can be executed on a single consumer-grade GPU (*e.g.*, RTX 3090 with 24 GB memory), showing strong practicality and deployment potential.

2. Related Work

2.1. Temporal Action Localization

Fully-Supervised Temporal Action Localization (FTAL), requires precise annotations of the start and end times of action instances in untrimmed videos. Similar to the categorization of object detection methods [19, 20], mainstream FTAL methods can be divided into one-stage and two-stage approaches based on the localization workflow. The one-stage methods [21, 8] utilize an end-to-end framework to locate and classify action instances in untrimmed videos. In contrast, the two-stage methods [22, 23], first densely generate proposals, then predict the categories of these proposals and adjust their boundaries. Although fully-supervised methods achieve impressive results, they rely on high-precision manual annotations, making them very costly.

Weakly-Supervised Temporal Action Localization (W-TAL) only uses video-level labels to detect action instances. Some Multiple Instance Learning (MIL) based methods [24] generate class activation sequences and localize action instances via threshold-based processing. Some other methods focus on feature learning to acquire more discriminative features. For example, Lee *et al.* [25] designs a network that reduces background noise to better identify the action instances in a video. Additionally, some efforts attempt to generate pseudo-labels to enhance supervision information. TSCN [26] creates frame-level pseudo-labels by blending attention sequences after considering

consensus from two sources. Although weakly-supervised methods significantly reduce annotation costs, they also hinder performance.

Point-Supervised Temporal Action Localization (PTAL) serves as a middle ground, bridging the gap between weak supervision and full supervision, while requiring only one-sixth the annotation time (30s *vs.* 300s per 1-min video) [14, 15] of fully supervised methods. SF-Net [14] first introduces single-frame supervision to the temporal action localization task, iteratively mining pseudo action frames and background frames to provide more supervision during training. Following this paradigm, numerous researchers study various optimization strategies. For instance, LACP [15] utilizes a greedy algorithm to generate densely optimized sequences, learning the completeness of action instances from point annotations. TSPNet [16] takes advantage of the prior knowledge that annotations are typically made at the center of action instances, developing a center scoring mechanism to improve localization accuracy. To address the issue of semantic ambiguity in determining action boundaries, Liu *et al.* [17] develops a step-by-step multi-grained boundary detection method to precisely locate action boundaries. Besides, HR-Pro [18] first generates more reliable proposals by learning discriminative snippet-level scores and adjusts these proposals through instance-level feature learning. However, these methods only focus on visual features, overlooking the text that could further enhance semantic information in complex scenes. In contrast to prior works, our proposed method effectively utilizes point annotations to refine the text and align various modalities, thereby boosting semantic information to improve the precision of localization.

2.2. Zero-Shot Image Captioning

Recently, zero-shot image captioning has gained more and more attention. Some methods [27, 28, 29] use a pre-trained vision-language model to guide the generation of a pre-trained LM. Specifically, ZeroCap [27] combines the CLIP [30] and GPT-2 [31] to generate image captions through the gradient-search iteration. On the other hand, Some methods [32, 33, 34] fine-tune a few parameters on large-scale data to facilitate better integration of image encoders with large language models. For example, BLIP-2 [32] employs a lightweight perceiver-based transformer (*i.e.*, Q-former) to bridge a

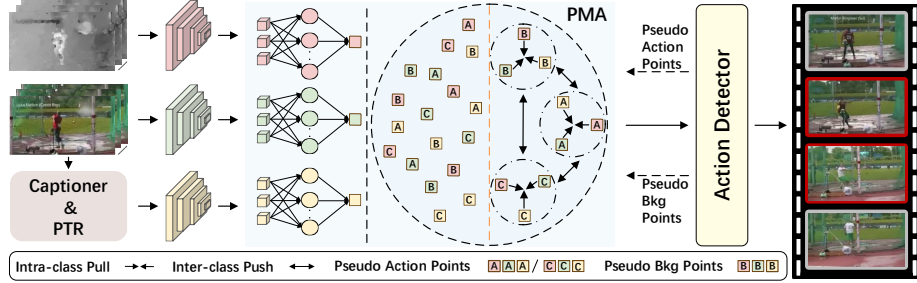


Figure 2: Overview of the proposed TRA. Differing from conventional methods that depend solely on visual features (such as RGB and optical flow), our method first employs a pre-trained captioner to generate relevant descriptions, then refines these descriptions through PTR, and maps all features to the same dimension using a linear layer. Subsequently, the detector’s predicted pseudo action and background points are used to select the corresponding features for contrastive learning, achieving feature alignment. Ultimately, the aligned features are fed into the action detector for localization. The detailed structure of PTR is provided in Sec. 3.1.

frozen visual encoder and a large language model. In this paper, we choose the widely-used BLIP2 as our caption generator.

3. Method

In this section, we first describe the task definition and present the overall architecture of our method. Then, we detail the point-based text refinement module (Sec. 3.1) and point-based multimodal alignment module (Sec. 3.2), respectively. In the end, we present the training and inference process in Sec. 3.3 and Sec. 3.4.

Task Definition Point-supervised Temporal Action Localization (PTAL) aims to learn a model using merely a single-frame annotation per action instance. Each action instance is annotated with a timestamp t and its category y . Given an untrimmed video, a trained PTAL model predicts actions in the form $(\hat{s}, \hat{e}, \hat{y}, \text{con})$, where \hat{s} and \hat{e} denote the start and end times of each predicted action instance, \hat{y} is the predicted action category, and con is the confidence score.

Method Overview The overall architecture of our TRA is shown in Fig. 2. Following previous works [18, 14, 15], we first segment the input video $V = \{I_i\}_{i=1}^M$, where I_i denotes the i -th frame and M is the total number of video frames, into T multi-frame snippets. A pre-trained video feature extractor (*i.e.*, I3D [35]) is employed to encode these snippets, thereby obtaining snippet-level visual features $\mathbf{F}_{\text{vision}}$, which consist of

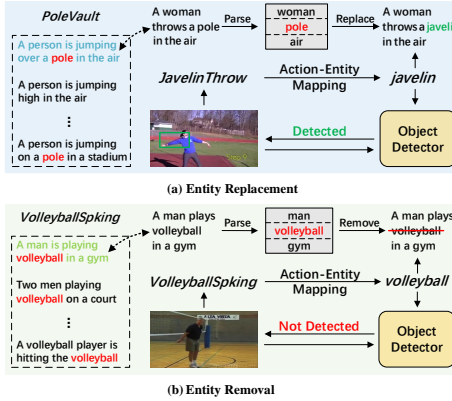


Figure 3: The proposed PTR module. (a) shows entity replacement, and (b) represents entity removal.

RGB features \mathbf{F}_{rgb} and optical flow features \mathbf{F}_{flow} . Meanwhile, we employ a pre-trained image captioner (*i.e.*, BLIP2 [32]) to generate a caption for each video frame. The initial captions sequence $\{s_i\}_{i=1}^M$ are then fed into our PTR module to obtain improved captions $\{\bar{s}_i\}_{i=1}^M$. Given that the frames within a snippet are highly similar to each other, we select the most frequently occurring frame description as the representation for each snippet. We further encode the snippet-level captions $\{\bar{s}_i\}_{i=1}^T$ using a pre-trained textual encoder (*i.e.*, XCLIP [36]) to generate textual features \mathbf{F}_{text} . Then, the \mathbf{F}_{vision} and \mathbf{F}_{text} are fed into our PMA module for alignment. The resulting aligned features are concatenated into $\hat{\mathbf{F}}$, which is subsequently fed into the action detector for temporal action localization. We adopt the best-performing HR-Pro [18] as our baseline.

In the following sections, we provide details of our PTR and PMA modules.

3.1. Point-based Text Refinement

In this section, we explain how the point-based text refinement module enhances the initially generated captions. First, we categorize actions by their dependency on entities and construct an action-to-entity mapping. Next, we analyze the flaws in initially generated descriptions, then identify specific video categories and extract the described entities. Subsequently, we build a reliable entity-dependent textual memory based on point annotations. Finally, we replace and remove incorrect entities. We provide details for each step below.

Action-to-Entity Mapping Construction. We divide actions into two categories: entity-dependent actions and entity-independent actions. Entity-dependent actions require specific entities to perform, such as *discus throw* (requires a *discus*). Conversely, entity-independent actions depend mainly on the body’s movements and do not need direct involvement with external entities, such as the *high jump* (which relies primarily on one’s own jumping ability). We identify the most relevant entity for each entity-dependent action, thereby constructing an action-entity mapping $\mathcal{M} : \{\text{action}_c \rightarrow \text{entity}_c\}_{c=1}^{C_e}$, where C_e is the number of entity-dependent action categories in the whole dataset. The specific details of mapping construction are in Sec. 4.1.

Flaws in Existing Descriptions. We observe that due to motion blur and background noise, the descriptions generated from video frames of entity-dependent actions are more likely to generate hallucinations, compared to those from entity-independent actions. For example, the description in Figure 3 (a) incorrectly identifies the “*hammer*” in the video as “*discus*”. In Figure 3(b), affected by the background, the captioner incorrectly describes “A man plays volleyball in a gym”. To minimize entity mistakes in these descriptions, we apply two operations: replacing or removing unreliable entities.

Video Classification and Entity Parsing. For an input video containing entity-dependent actions, its entity-dependent action labels are denoted as $\{\text{y}_c\}_{c=1}^{C_v}$, where C_v is the number of entity-dependent action categories in the video. For training videos, we directly use the annotated video-level labels, while for testing videos, we classify them using the trained baseline action detector. Based on \mathcal{M} , we denote the set of entity categories associated with a specific video as $E_v = \{e_c\}_{c=1}^{C_v}$, and the complete set of entity categories in the dataset as E_e . The complement set E_x contains entities in E_e that do not appear in E_v . We use an off-the-shelf textual parser, *TextGraphParser* [37], to extract the relevant entities from each caption. Formally, the process is represented as $s_i \mapsto \{e_{ij}\}_{j=1}^{k_i}$, where e_{ij} denotes the j -th entity in the i -th caption, and k_i is the total number of entities extracted from that caption.

Build Entity-Dependent Memory. We construct a point annotations-based memory as a reference, to evaluate whether a caption describes an action frame. In the point annotation setting, each annotation corresponds to an action category, and a subset of the annotations is related to entity-dependent actions. For these entity-dependent

annotations, we also collect the associated descriptions of the annotated frames. Since some annotated frame descriptions may contain mismatched entity noise as previously mentioned, we filter out these incorrect descriptions and use the rest to build a reliable entity-dependent textual memory \mathbb{M} . $\mathbb{M}(y)$ denotes the set of point-level descriptions associated with the action category y .

Entity Replacement. The generated descriptions with mismatched entities can mislead the model, so we replace them with the correct ones. If an entity in a sentence belongs to the irrelevant entity set E_x , it is necessary to determine whether the sentence describes the action or the background. Note that background frames may also contain entities in E_x . For instance, a discus and a hammer may both be present on the ground, but the player only throws the hammer. Therefore, irrelevant entities are permitted in background descriptions. After locating the sentence s_i containing $e_{ij} \in E_x$, we leverage a text embedding model Angle to calculate the semantic similarity between s_i and each annotated sentence m in $\mathbb{M}(y_{e_{ij}})$.

$$sim(s_i, \mathbb{M}(y_{e_{ij}})) = \max_{m \in \mathbb{M}(y_{e_{ij}})} \cos(\text{Angle}(s_i), \text{Angle}(m)) \quad (1)$$

where \cos represents the cosine similarity, $y_{e_{ij}}$ represents the action category of e_{ij} .

If $sim(s_i, \mathbb{M}(y_{e_{ij}}))$ exceeds the predefined threshold θ_1 , s_i requires entity adjustment. Each e_v in E_v and the frame I_i associated with s_i are jointly fed into the open-set object detector OWLv2 [38], which predicts the corresponding coordinate loc_{e_v} and confidence score $score_{e_v}$:

$$(loc_{e_v}, score_{e_v}) = Det(e_v, I_i) \quad (2)$$

where Det represents the entity detection process. We then identify the entity \hat{e}_v with the highest confidence:

$$\hat{e}_v = \arg \max_{e_v \in E_v} score_{e_v} \quad (3)$$

Finally, the mismatched entity e_{ij} in sentence s_i is replaced with \hat{e}_v , yielding the updated sentence \hat{s}_i .

Entity Removal. After fixing mismatched entities, we further remove those entities that appear in the action descriptions but not in the video frames. Similar to entity

replacement, we focus on the action descriptions. Because the video frame background might contain some title cards, such as “volleyball from approach and arm swing”, the term ‘volleyball’ refers to text, not an actual volleyball, and it should not be deleted. Specifically, we identify the sentence \hat{s}_i containing $e_{ij} \in E_v$ and use AnglE to compute the semantic similarity between \hat{s}_i and the annotated sentences m in $\mathbb{M}(y_{e_v})$.

$$sim(\hat{s}_i, \mathbb{M}(y_{e_v})) = \max_{m \in \mathbb{M}(y_{e_v})} \cos(\text{Angle}(\hat{s}_i), \text{Angle}(m)) \quad (4)$$

Similar to entity replacement, if $sim(\hat{s}_i, \mathbb{M}(y_{e_v}))$ exceeds the threshold θ_2 , e_{ij} and I_i are passed into OWLv2 to generate the coordinates $loc_{e_{ij}}$ and confidence scores $score_{e_{ij}}$:

$$(loc_{e_{ij}}, score_{e_{ij}}) = Det(e_{ij}, I_i) \quad (5)$$

If $score_{e_{ij}}$ falls below γ , e_{ij} is considered undetected and is removed from \hat{s}_i ; otherwise, no modification is applied. After removing low-confidence entities (*i.e.*, those with $score_{e_{ij}} < \gamma$), we obtain the final refined caption, denoted as \bar{s}_i . For brevity, we describe the entity replacement and removal as Algorithm 1.

3.2. Point-based Multimodal Alignment

After enhancing the initial captions using PMA, we perform feature alignment between the text features and vision features (RGB and optical flow). Specifically, the three feature types are projected by separate linear layers into a common feature dimension D :

$$\begin{aligned} \hat{\mathbf{F}}_{text} &= \text{MLP}_{text}(\mathbf{F}_{text}) \\ \hat{\mathbf{F}}_{rgb} &= \text{MLP}_{rgb}(\mathbf{F}_{rgb}) \\ \hat{\mathbf{F}}_{flow} &= \text{MLP}_{flow}(\mathbf{F}_{flow}) \end{aligned} \quad (6)$$

where $\hat{\mathbf{F}}_{text}$, $\hat{\mathbf{F}}_{rgb}$, and $\hat{\mathbf{F}}_{flow} \in \mathbb{R}^{T \times D}$. By leveraging N_{act} pseudo action points and N_{bkg} pseudo background points predicted by the action detector, we perform contrastive learning to minimize intra-class distance and maximize inter-class distance. The text-

Algorithm 1 Captions Refinement.

Input: Initial captions sequence $\{s_i\}_{i=1}^M$, initial entities sequence $\{e_{ij}\}_{j=1}^{k_i}\}_{i=1}^M$, video

frames sequence $\{I_i\}_{i=1}^M$.

Output: Refined captions sequence $\{\bar{s}_i\}_{i=1}^M$.

```

1: for  $i = 1$  to  $M$  do
2:   for  $j = 1$  to  $k_i$  do
3:     if  $e_{ij} \in E_x$  and  $sim(s_i, \mathbb{M}(y_{e_{ij}})) > \theta_1$ , then
4:        $(loc_{e_v}, score_{e_v}) = Det(e_v, I_i), \forall e_v \in E_v$ 
5:        $\hat{e}_v = \arg \max_{e_v \in E_v} score_{e_v}$ 
6:       Replace  $e_{ij}$  with  $\hat{e}_v$ 
7:     end if
8:   end for
9:    $\hat{s}_i \leftarrow \{e_{i1}, e_{i2}, \dots, e_{ik_i}\}$ 
10:  for  $j = 1$  to  $k_i$  do
11:    if  $e_{ij} \in E_v$  and  $sim(\hat{s}_i, \mathbb{M}(y_{e_v})) > \theta_2$ , then  $(loc_{e_{ij}}, score_{e_{ij}}) = Det(e_{ij}, I_i)$ 
12:      if  $score_{e_{ij}} < \gamma$ , then Remove  $e_{ij}$  from  $\hat{s}_i$ 
13:      end if
14:    end if
15:    $\bar{s}_i \leftarrow \{e_{i1}, e_{i2}, \dots, e_{im_i}\} (m_i \leq k_i)$ 
16: end for
17: Return  $\{\bar{s}_i\}_{i=1}^M$ 

```

to-vision contrastive loss \mathcal{L}_{t2v} is calculated as:

$$\mathcal{L}_{t2v} = -\frac{1}{2N} \sum_{i=1}^N \sum_{j=1}^N \mathbb{I}_{[y_i=y_j]} (\log \frac{\langle \hat{\mathbf{f}}_i^{text}, \hat{\mathbf{f}}_j^{rgb} \rangle}{\sum_{k=1}^N \langle \hat{\mathbf{f}}_i^{text}, \hat{\mathbf{f}}_k^{rgb} \rangle} + \log \frac{\langle \hat{\mathbf{f}}_i^{text}, \hat{\mathbf{f}}_j^{flow} \rangle}{\sum_{k=1}^N \langle \hat{\mathbf{f}}_i^{text}, \hat{\mathbf{f}}_k^{flow} \rangle}) \quad (7)$$

and the vision-to-text contrastive loss \mathcal{L}_{v2t} :

$$\mathcal{L}_{v2t} = -\frac{1}{2N} \sum_{i=1}^N \sum_{j=1}^N \mathbb{I}_{[y_i=y_j]} (\log \frac{\langle \hat{\mathbf{f}}_i^{rgb}, \hat{\mathbf{f}}_j^{text} \rangle}{\sum_{k=1}^N \langle \hat{\mathbf{f}}_i^{rgb}, \hat{\mathbf{f}}_k^{text} \rangle} + \log \frac{\langle \hat{\mathbf{f}}_i^{flow}, \hat{\mathbf{f}}_j^{text} \rangle}{\sum_{k=1}^N \langle \hat{\mathbf{f}}_i^{flow}, \hat{\mathbf{f}}_k^{text} \rangle}) \quad (8)$$

where $N = N_{act} + N_{bkg}$, \mathbb{I} represents the indicator function, and $\langle \cdot, \cdot \rangle$ is the similarity function formulated as $\langle \mathbf{x}_1, \mathbf{x}_2 \rangle = \exp(\mathbf{x}_1 \cdot \mathbf{x}_2 / \tau)$ with a temperature parameter τ . The total objective function of the PMA module is described as:

$$\mathcal{L}_{pma} = \frac{1}{2} \mathcal{L}_{t2v} + \frac{1}{2} \mathcal{L}_{v2t}. \quad (9)$$

3.3. Training

Our full framework is trained end-to-end by optimizing the sum of all loss terms:

$$\mathcal{L}_{total} = \mathcal{L}_{base} + \lambda \mathcal{L}_{pma}, \quad (10)$$

where \mathcal{L}_{base} represents the original loss function of the base action detector, λ is a trade-off hyperparameter. More details of \mathcal{L}_{base} are given in Sec. 4.1.

3.4. Inference

The multi-modal features $\hat{\mathbf{F}} = \text{Concat}(\hat{\mathbf{F}}_{rgb}, \hat{\mathbf{F}}_{flow}, \hat{\mathbf{F}}_{text})$ are fed into the action detector to generate a series of proposals. Finally, we use Soft-NMS [39] to remove overlapping proposals.

4. Experiment

4.1. Experimental Setup

Dataset. In this paper, we conduct experiments on five widely used PTAL benchmarks. **THUMOS’14** [59] is a widely used challenging dataset for Temporal Action Localization. It contains 413 untrimmed sports videos, covering 20 action categories with an average of 15 action instances per video. Following standard divisions, we use 200 videos for training and 213 videos for testing. **BEOID** [60] provides 58 video samples with 34 operation classes in 6 locations, including 46 videos for training and 12 videos for testing. **GTEA** [21] includes 28 untrimmed videos of 7 fine-grained daily activities in a kitchen. We adopt the standard split, which involves using 21 videos for training, and 7 videos for testing. **ActivityNet** [61] is a large-scale dataset designed for action detection and offers two different versions. Version 1.3 includes 10,024 training videos,

Supervision	Method	mAP@IoU (%)							AVG (0.1:0.5)	AVG (0.3:0.7)	AVG (0.1:0.7)
		0.1	0.2	0.3	0.4	0.5	0.6	0.7			
Frame-level (Full)	P-GCN [40] (ICCV'19)	69.5	67.8	63.6	57.8	49.1	-	-	61.6	-	-
	TCANet [41] (CVPR'21)	-	-	60.6	53.2	44.6	36.8	26.7	-	44.3	-
	BMN+CSA [42] (ICCV'21)	-	-	64.4	58.0	49.2	38.2	27.8	-	47.5	-
	GCM [43] (TPAMI'21)	72.5	70.9	66.5	60.8	51.9	-	-	64.5	-	-
	VSGN [44] (ICCV'21)	-	-	66.7	60.4	52.4	41.0	30.4	-	50.2	-
	AFSD [45] (CVPR'21)	-	-	67.3	62.4	55.5	43.7	31.1	-	52.0	-
Video-level (Weak)	ACG-Net [46] (AAAI'22)	68.1	62.6	53.1	44.6	34.7	22.6	12.0	52.6	33.4	42.5
	RSKP [47] (CVPR'22)	71.3	65.3	55.8	47.5	38.2	25.4	12.5	55.6	35.9	45.1
	DELU [48] (ECCV'22)	71.5	66.2	56.5	47.7	40.5	27.2	15.3	56.5	37.4	46.4
	P-MIL [24] (CVPR'23)	71.8	67.5	58.9	49.0	40.0	27.1	15.1	57.4	38.0	47.0
	Zhou <i>et al.</i> [49] (CVPR'23)	74.0	69.4	60.7	51.8	42.7	26.2	13.1	59.7	38.9	48.3
	PivoTAL [50] (CVPR'23)	74.1	69.6	61.7	52.1	42.8	30.6	16.7	60.1	40.8	49.6
	ISSF [51] (AAAI'24)	72.4	66.9	58.4	49.7	41.8	25.5	12.8	57.8	37.6	46.8
	PVLR [52] (MM'2024)	74.9	69.9	61.4	53.1	45.1	30.5	17.1	60.9	-	50.3
Point-level (Weak)	ARST [53] (CVPR'19)	24.3	19.9	15.9	12.5	9.0	-	-	16.30	-	-
	SF-Net [14] (ECCV'20)	68.3	62.3	52.8	42.2	30.5	20.6	12.0	51.2	31.6	41.2
	LACP [15] (ICCV'21)	75.7	71.4	64.6	56.5	45.3	34.5	21.8	62.7	44.5	52.8
	BackTAL [54] (TPAMI'21)	-	-	54.4	45.5	36.3	26.2	14.8	-	35.4	-
	CRRC-Net [55] (TIP'22)	77.8	73.5	67.1	57.9	46.6	33.7	19.8	64.6	45.1	53.8
	SMBD [17] (ECCV'24)	-	-	66.0	57.9	47.0	36.0	22.0	64.2	45.7	-
	SNPR [56] (TIP'24)	77.9	73.9	66.6	59.4	48.6	36.7	22.7	65.3	46.8	55.1
	AAPL [57] (AAAI'25)	64.3	-	54.6	-	35.2	-	14.0	-	-	42.8
	TRA (Ours)	83.6	79.4	71.6	62.0	51.4	37.6	23.7	69.6^{†4.3}	49.3^{†2.5}	58.5^{†3.4}
	DCM [58] (ICCV'21)	72.3	64.7	58.2	47.1	35.9	23.0	12.8	55.6	35.4	44.9
Point-level (Full)	TSPNet [16] (CVPR'24)	82.3	77.6	70.1	60.0	49.4	37.6	24.5	67.9	48.3	57.4
	HR-Pro [18] (AAAI'24)	85.6	81.6	74.3	64.3	52.2	39.8	24.8	71.6	51.1	60.3
	TRA* (Ours)	86.6	83.6	76.3	66.7	55.2	41.4	26.5	73.7^{†2.1}	53.2^{†2.1}	62.3^{†2.0}

Table 1: Comparison with the state-of-the-art methods on THUMOS'14. We also compare the method with fully-supervised and weakly-supervised methods. We use the same point annotations as [15]. \uparrow highlights the absolute performance improvement between the best and second-best methods in point-level supervision. To compare fairly with proposal-based refinement methods [16, 18, 58], we also employ a proposal-based boundary adjustment, similar to [18]. * represents our proposal-based results.

4,926 validation videos, and 5,044 test videos, divided into 200 action categories. Version 1.2, a subset of version 1.3, consists of 4,819 training videos, 2,383 validation videos, and 2,480 test videos, covering 100 action categories. We conduct experiments on both versions of ActivityNet to validate the generalization of our approach.

Evaluation Metrics. We follow the standard protocol to evaluate the action localization performance across three datasets using mean Average Precision (mAP) at different Intersection-over-Union (IoU) thresholds. A proposal is considered positive only if it exceeds the specified IoU threshold and the correct category prediction.

Implementation Details. Following [15, 14, 18], we split each video into non-overlapping 16-frame snippets and use the TV-L1 algorithm to extract optical flow. For a fair comparison, we also follow the previous works to use a two-stream I3D [35] network pre-trained on Kinetics-400 to extract the visual features. The sentence similarity threshold θ_1 and θ_2 are set to 0.4 and 0.75, respectively. The detection threshold of OWL_{v2} is set to 0.1. In the training, the balance factor λ is set to 0.9, the temperature parameter τ is

Dataset	Method	mAP@IoU (%)				AVG (0.1:0.7)
		0.1	0.3	0.5	0.7	
GTEA	SF-Net [14] (ECCV’20)	58.0	37.9	19.3	11.9	31.0
	LACP [15] (ICCV’21)	63.9	55.7	33.9	20.8	43.5
	SMBD [17] (ECCV’24)	75.0	61.3	41.1	14.2	47.4
	SNPR [56] (TIP’24)	74.3	62.8	35.7	13.7	46.6
	AAPL [57] (AAAI’25)	70.3	54.4	37.7	23.4	46.3
	TRA	76.0	66.0	46.8	22.0	52.8^{↑5.4}
	DCM [58] (ICCV’21)	59.7	38.3	21.9	18.1	33.7
	TSPNet [16] (CVPR’24)	74.6	60.9	39.5	16.6	49.0
	HR-Pro [18] (AAAI’24)	72.6	61.1	37.3	17.5	47.3
BEOID	TRA* (Ours)	77.9	67.8	47.2	22.4	54.1^{↑5.1}
	SF-Net [14] (ECCV’20)	62.9	40.6	16.7	3.5	30.9
	LACP [15] (ICCV’21)	76.9	61.4	42.7	25.1	51.8
	BackTAL [54] (TPAMI’21)	60.1	40.9	21.2	11.0	32.5
	SMBD [17] (ECCV’24)	78.2	71.0	52.5	25.2	57.4
	SNPR [56] (TIP’24)	77.2	64.3	44.0	24.5	53.1
	AAPL [57] (AAAI’25)	75.5	67.6	48.5	26.3	55.2
	TRA	82.1	71.0	55.1	30.0	60.8^{↑3.4}
	DCM [58] (ICCV’21)	63.2	46.8	20.9	5.8	34.9
	TSPNet [16] (CVPR’24)	83.8	73.0	51.1	23.8	59.6
	HR-Pro [18] (AAAI’24)	78.5	72.1	55.3	26.1	59.4
	TRA* (Ours)	83.3	74.5	58.9	31.4	63.7^{↑4.1}

Table 2: Comparison results with the state-of-the-art methods on GTEA and BEOID. \uparrow represents the absolute gain between the best and second-best PTAL methods. We make the same proposal-based boundary adjustment [18] for a fair comparison with two-stage methods [16, 18, 58]. * denotes our refinement results.

set to 1.0, the learning rate is set to 0.0002, and other parameters (*e.g.*, batch size) are maintained as in the baseline. Our entire framework is implemented with PyTorch and all experiments are conducted on $1 \times$ RTX-3090Ti GPU.

Specific Pre-trained Models We use several pre-trained models throughout the pipeline to achieve our goal. Specifically, We use the pre-trained BLIP¹ [32] as our caption generator, which is fine-tuned on web-scale image-text datasets (*e.g.*, LAION [62]) and has strong zero-shot image captioning abilities. The pre-trained XCLIP² [36] is employed to extract the text features, which is pre-trained on large-scale action recognition Kinetics-400 [63] dataset and provides powerful representation for action-related sentences. The pre-trained TextGraphParser³ [37] serves as the sentence parser to extract entities, which is fine-tuned on FACTUAL [37] scene graph parsing dataset and can

¹<https://huggingface.co/Salesforce/blip2-opt-6.7b>

²<https://huggingface.co/microsoft/xclip-base-patch16-16-frames>

³<https://huggingface.co/lizhuang144/flan-t5-base-VG-factual-sg>

Dataset	Method	mAP@IoU (%)			AVG (0.5:0.95)
		0.5	0.75	0.95	
ActivityNet1.2	SF-Net [14] (ECCV’20)	37.8	-	-	22.8
	LACP [15] (ICCV’21)	44.0	26.0	5.9	26.1
	BackTAL [54] (TPAMI’21)	41.5	27.3	4.7	27.0
	SNPR [56] (TIP’24)	43.4	31.3	5.4	27.5
	TRA	46.8	27.3	6.7	28.4
	TRA* (Ours)	49.6	29.0	7.3	30.2
ActivityNet1.3	LACP [15] (ICCV’21)	40.4	24.6	5.7	25.1
	CRRC [55] (TIP’22)	39.8	24.1	5.9	24.0
	SNPR [56] (TIP’24)	41.3	30.9	4.8	26.5
	AAPL [57] (AAAI’25)	39.6	24.3	5.6	24.7
	TRA	43.9	26.4	6.5	27.1
	HR-Pro [18] (AAAI’24)	42.8	27.2	8.0	27.1
	TRA* (Ours)	45.3	27.4	6.8	28.0

Table 3: Comparison results with the state-of-the-art methods on ActivityNet1.2 and ActivityNet1.3. * denotes our boundary adjustment results, identical to the proposal-based refinements in [18].

capture the accuracy entities from the given sentence. We leverage the OWLv2⁴ [38] to detect if the key entities are in the video frames, which uses CLIP [30] as its multi-modal backbone and has the excellent zero-shot text-conditioned object detection ability. Angle⁵ [64] demonstrates state-of-the-art (SOTA) performance on semantic textual similarity tasks, so we use it to compute the similarity between the generated caption and entity-dependent memory. The aforementioned pre-trained models are publicly and readily available.

Action-Entity Mapping Construction The construction of action-entity mapping consists of two steps: (1) Using a large language model to automatically classify action categories and identify related entities according to the predefined standards in Sec. 3.1, and (2) Manually adjusting the above results to guarantee accuracy. In detail, we use ChatGPT-4⁶ to build the action-entity mapping, as shown in Fig. 4. Due to the hallucination and randomness inherent in large language models, we manually adjust the initially generated results. The final action-entity mapping we used is shown in Table 4.

Base Loss of Action Detector In Sec. 3.3, we use the original loss function of the

⁴<https://huggingface.co/google/owlv2-large-patch14-ensemble>

⁵<https://huggingface.co/WhereIsAI/UAE-Large-V1>

⁶<https://openai.com>

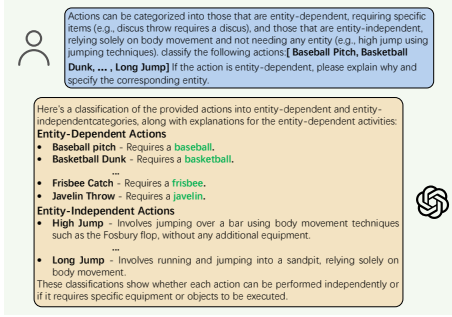


Figure 4: Using ChatGPT-4 to construct the action-entity mapping.

Action-Entity Mapping		
Number	Action	Entity
1	Baseball Pitch	baseball
2	Basketball Dunk	basketball
3	Billiards	billiard ball
4	Clean and Jerk	barbell
5	Cricket Bowling	cricket ball
6	Cricket Shot	cricket bat
7	Golf Swing	golf club
8	Harmer Throw	harmer
9	Pole Vault	pole
10	Soccer Penalty	soccer ball
11	Tennis Swing	tennis racket
12	Shot Put	shot
13	Throw Discus	discus
14	Volleyball Spiking	volleyball
15	Frisbee Catch	frisbee
16	Javelin Throw	javelin
17	High Jump	-
18	Cliff Diving	-
19	Diving	-
20	Long Jump	-

Table 4: The specific action-entity mapping.

baseline as \mathcal{L}_{base} . Taking the baseline HR-Pro [18] as an example, \mathcal{L}_{base} consists of the frame-wise loss function \mathcal{L}_{frame} and the feature-wise loss function $\mathcal{L}_{feature}$:

$$\mathcal{L}_{base} = \mathcal{L}_{frame} + \mathcal{L}_{feature} \quad (11)$$

where

$$\mathcal{L}_{frame} = \frac{1}{N_{act}} \sum_{c=1}^C \sum_{t \in \mathcal{T}^+}^{N_{act}} FL(\mathbf{P}_{t,c}) + \frac{1}{N_{bkg}} \sum_{t \in \mathcal{T}^-}^{N_{bkg}} FL(1 - \mathbf{A}_t) \quad (12)$$

N_{act} and N_{bkg} is the total number of pseudo action snippets \mathcal{T}^+ and background snippets

\mathcal{T}^- respectively, \mathbf{P} and \mathbf{A} are the snippet-level prediction and class-agnostic attention sequence, C represents the number of total action classes, FL represents the focal loss function [65].

$$\begin{aligned} \mathcal{L}_{feature} = & -\frac{1}{C} \sum_{c=1}^C \sum_{t_i^c} \log \left(\frac{\langle \bar{\mathbf{x}}_{t_i^c} \cdot \bar{\mathbf{m}}_c \rangle}{\langle \bar{\mathbf{x}}_{t_i^c} \cdot \bar{\mathbf{m}}_c \rangle + \sum_{k \neq c} \langle \bar{\mathbf{x}}_{t_i^c} \cdot \bar{\mathbf{m}}_k \rangle} \right. \\ & \left. + \frac{\langle \bar{\mathbf{x}}_{t_i^c} \cdot \bar{\mathbf{m}}_c \rangle}{\langle \bar{\mathbf{x}}_{t_i^c} \cdot \bar{\mathbf{m}}_c \rangle + \sum_{\forall t_j \in \mathcal{T}^-} \langle \bar{\mathbf{x}}_{t_j} \cdot \bar{\mathbf{m}}_c \rangle} \right) \end{aligned} \quad (13)$$

where t_i^c indicates the pseudo action snippet of class c , $\bar{\mathbf{x}}$ represent the normalized embedded snippet features, $\bar{\mathbf{m}}_c$ represent the normalized prototype of class c , $\langle \cdot, \cdot \rangle$ is the same similarity operation in Sec. 3.3.

4.2. Comparison with State-of-The-Art Methods

In Table 1, we evaluate our TRA against several state-of-the-art methods under different levels of supervision on THUMOS’14. Our model achieves the best performance among all point-level and video-level weakly-supervised approaches. In snippet-level approaches, our method outperforms the second-ranked SNPR, achieving absolute improvements of 4.3%, 2.5%, and 3.4% on the metrics of average mAP (0.1:0.5), average mAP (0.3:0.7), and average mAP (0.1:0.7) respectively. Compared to PTAL methods that perform boundary adjustment in the second phase, our proposal-based refinement TRA reaches an average mAP (0.1:0.7) of 62.3%, leading by about 2.0% over the previous best result. When compared with some fully supervision methods, such as AFSD, our method still shows a superior performance (53.2% v.s. 52.0% in average mAP for IoU thresholds of 0.3:0.7). Table 2 demonstrates the impressive performance of our method on the GTEA and BEOID benchmarks. In both datasets, our method gains an absolute improvement of 5.4% and 3.4% in terms of average mAP (0.1:0.7), while the proposal-based refinement surpasses comparable methods by 5.1% and 4.1%. Given that both datasets consist of ego-centric daily activities rather than complex sports actions, we remove the PTA module. We also evaluate our method on large-scale action detection datasets. As shown in Table 3, our method achieves the best performance on both the ActivityNet 1.2 and ActivityNet 1.3 large-scale datasets, with 30.2% mAP and 28.0% mAP, respectively.

Method	mAP@IoU(%)				
	0.1	0.3	0.5	0.7	AVG
LACP [‡]	75.3	64.3	45.1	20.6	52.4
LACP + Ours	79.1	67.8	45.4	20.8	54.1 ^{†1.7}
HR-Pro [‡] _{snippet}	82.0	69.4	48.2	21.9	56.2
HR-Pro _{snippet} + Ours	83.6	71.6	51.4	23.7	58.5 ^{†2.3}

Table 5: Results of incorporating TRA into different PTAL methods on THUMOS’14. [‡] represents our reproduced results.

Setup			AVG mAP@IoU(%)		
TEXT	PTR	PMA	[0.1:0.5]	[0.3:0.7]	[0.1:0.7]
✗	✗	✗	67.4	46.9	56.2
✓	✗	✗	68.0	47.5	56.9
✓	✓	✗	68.8	48.2	57.6
✓	✓	✓	69.6^{†2.2}	49.3^{†2.4}	58.5^{†2.3}

Table 6: Ablation study on THUMOS14. [†] denotes the relative gain between our full model and baseline.

4.3. Generalization

To validate the generalization of our method, we plug our proposed module into two different state-of-the-art base action locators. The results in Table 5 demonstrate that our method achieves improvements across different baselines, indicating its generalizability. We observe that our method brings more performance improvements to HR-Pro compared to LACP. This is because a stronger baseline generates more accurate pseudo action points and background points, resulting in greater enhancements to the PMA.

4.4. Ablation Study

In this section, we perform a set of ablation studies on THUMOS’14 as it is the most challenging.

Effectiveness of Each Component. Table 6 presents the comparison results of using different modules of TRA. The first line represents the baseline, which uses only visual features without any extra modules, achieving an average mAP (0.1:0.7) of 56.2%. Incorporating the initial text modality generated by BLIP2 leads to a 0.7% increase in average mAP for IoU thresholds of 0.1:0.7 (Row 2 v.s. Row 1). By augmenting the original caption with the proposed PTA, the model realizes a further increase in performance, reaching an average mAP (0.1:0.7) of 57.6% (the third row). Following the alignment of visual and textual modalities through PMA, our full model achieves the

Model	Pre-trained	Fine-tune	AVG mAP@IoU(%)			
			[0.1:0.5]	[0.3:0.7]	[0.1:0.7]	
CLIP-VIT B/32	WIT-400M	-	67.7	46.7	56.3	
XCLIP-VIT B/32	WIT-400M	Kinetics-400	68.5	48.1	57.4	
CLIP-VIT B/16	WIT-400M		68.9	48.3	57.7	
XCLIP-VIT B/16	WIT-400M	Kinetics-400	69.6	49.3	58.5	

Table 7: Performance with different Caption Feature Extractor.

Model	#Params	mAP@IoU(%)				
		0.1	0.3	0.5	0.7	AVG
BLIP2-OPT _{2.7B}	3.8B	83.0	71.3	50.6	22.2	57.8
BLIP2-Flan-T5 _{xl}	4.1B	82.8	71.2	49.5	22.7	57.7
BLIP2-OPT _{6.7B}	7.8B	83.6	71.6	51.4	23.7	58.5

Table 8: Performance with different configuration BLIP2.

best average mAP (0.1:0.7) with a score of 58.5%, surpassing the visual-only baseline by 2.3% (Row 3 *v.s.* Row 4). This clearly shows that our proposed modules enhance and complement precise action localization.

Effect of Different Caption Feature Extractor. In Table 7, we compare the performance of our method under different caption feature extractors. We observe that VIT-B/16 outperforms VIT-B/32 when used as the backbone (Row 1 *v.s.* Row 3 & Row 2 *v.s.* Row 4), primarily because it can capture more fine-grained features. We also notice that fine-tuning on the Kinetics-400 dataset leads to better performance, as it is a large action recognition dataset. Overall, using XCLIP-VIT B/16 as the text feature extractor achieves superior performance.

Impact of Caption Quality. In order to study the impact of caption quality on our method, we use different configurations of BLIP2 as the captioner to generate captions of different quality. The results are present in Table 8. We observe that when BLIP2 utilizes the OPT with 6.7 B parameters as the language model, it achieves the best average mAP on various IoU thresholds. It might be attributed to its sufficient amount of parameters, leading to higher-quality caption generation. For this reason, we choose it as our caption generator.

Influence of Different Entity Detection Threshold. The entity detection threshold γ can partially affect detection performance as shown in Figure 5. Both overly high and overly low entity detection thresholds can degrade the performance. This is because a too-high threshold may ignore key entities, while a too-low threshold could introduce

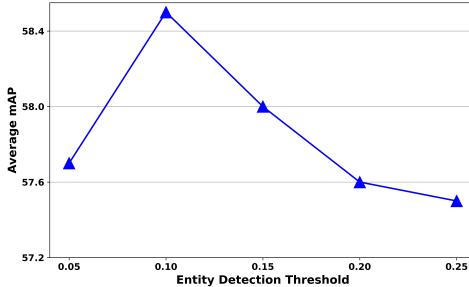


Figure 5: Performance comparison (Average mAP for IoU thresholds of 0.1:0.7) under different entity detection thresholds.

noisy entities (e.g., circular lights on a volleyball court).

4.5. Discussion on Computational Cost

Table 9: Computational cost analysis of each pre-trained model during inference (including GPU memory usage from model parameters and forward propagation), measured in MB on an RTX 3090.

Model	BLIP2	TextGraphParser	OWLv2	AngLE	XCLIP
GPU Memory Usage (MB)	16656	2158	8492	2374	2760

Our framework involves several pre-trained models for textual semantic enhancement compared to the baseline, resulting in a certain increase in computational cost. Table 9 presents the GPU memory usage of each pre-trained model during inference, ranging from 2158MB to 16656MB. However, these pre-trained models are invoked sequentially rather than concurrently. As a result, the entire pipeline can be executed on a single GPU, such as a consumer-grade RTX 3090 with 24GB of memory, making the overall computational cost manageable and acceptable.

4.6. Qualitative Results

Qualitative Comparison. In Figure 6, we compare the qualitative result of our method with HR-Pro on test videos in THUMOS’14. Figure 6 (a) shows that our model provides more precise localization for action instances. It is evident that HR-Pro ignores the first action instance, while the second instance is predicted incompletely, with some parts missing. By contrast, our method detects more complete snippets and achieves clearer boundaries than HR-Pro. In Figure 6 (b), HR-Pro incorrectly divides the second

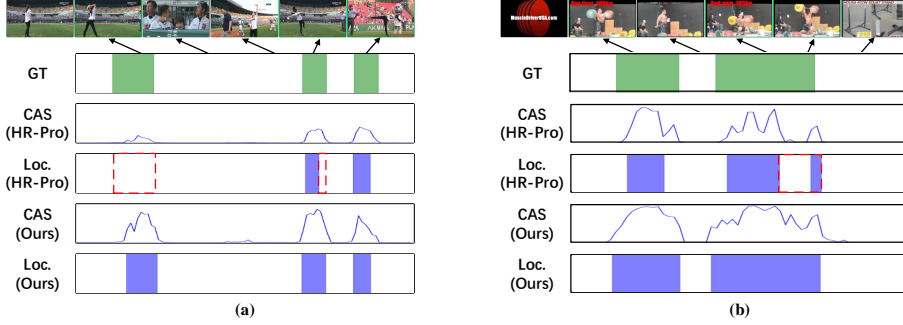


Figure 6: Qualitative comparison between our proposed method and HR-Pro [18] on THUMOS’14. We present two examples from different action classes: (1) BaseballPitch and (2) CleanAndJerk. The first row displays the input video, followed by the second row showing the ground-truth intervals. The third and fourth rows present the class-specific activation sequence (CAS) and localization results from HR-Pro, respectively. The fifth and sixth rows show our CAS and localization results. Red boxes indicate false positives or missed action detections. Our detection results have notably higher IoUs with the ground truths.

action instance into two parts, whereas our method successfully detects the complete instance.

5. Conclusion

This paper proposes a novel TRA framework for point-supervised temporal action localization, which plugs the refined captions and aligns visual and linguistic modalities to enhance semantic information for better localization results. The proposed PTR takes the descriptions generated from point annotations as a reference and leverages several pre-trained models to adjust the initially inaccurate descriptions. Subsequently, the PMA uses the pseudo-point labels predicted by the detector to align multiple modalities features. Extensive experiments on five benchmarks demonstrate that TRA significantly outperforms existing PTAL methods and achieves state-of-the-art results, which validates the effectiveness of our approach.

References

[1] T. Yao, T. Mei, Y. Rui, Highlight detection with pairwise deep ranking for first-person video summarization, in: CVPR, IEEE Computer Society, 2016.

- [2] S. Vishwakarma, A. Agrawal, A survey on activity recognition and behavior understanding in video surveillance, *The Visual Computer* 29 (10) (2013) 983–1009.
- [3] H. Alwassel, F. C. Heilbron, B. Ghanem, Action search: Spotting actions in videos and its application to temporal action localization, in: *ECCV*, Springer, 2018.
- [4] Z. Qing, H. Su, W. Gan, D. Wang, W. Wu, X. Wang, Y. Qiao, J. Yan, C. Gao, N. Sang, Temporal context aggregation network for temporal action proposal refinement, in: *CVPR*, 2021, pp. 485–494.
- [5] X. Wang, H. Zhang, S. Zhang, C. Gao, Y. Shao, N. Sang, Context-aware proposal network for temporal action detection, *arXiv preprint arXiv:2206.09082* (2022).
- [6] Q. Wang, Y. Zhang, Y. Zheng, P. Pan, Rcl: Recurrent continuous localization for temporal action detection, in: *CVPR*, 2022, pp. 13566–13575.
- [7] S. Nag, X. Zhu, Y.-Z. Song, T. Xiang, Proposal-free temporal action detection via global segmentation mask learning, in: *ECCV*, 2022, pp. 645–662.
- [8] C.-L. Zhang, J. Wu, Y. Li, Actionformer: Localizing moments of actions with transformers, in: *ECCV*, 2022, pp. 492–510.
- [9] L. Wang, Y. Xiong, D. Lin, L. Van Gool, Untrimmednets for weakly supervised action recognition and detection, in: *CVPR*, 2017, pp. 4325–4334.
- [10] Z. Shou, H. Gao, L. Zhang, K. Miyazawa, S.-F. Chang, Autoloc: Weakly-supervised temporal action localization in untrimmed videos, in: *ECCV*, 2018, pp. 154–171.
- [11] Z. Liu, L. Wang, Q. Zhang, Z. Gao, Z. Niu, N. Zheng, G. Hua, Weakly supervised temporal action localization through contrast based evaluation networks, in: *ICCV*, 2019, pp. 3899–3908.
- [12] P. Lee, Y. Uh, H. Byun, Background suppression network for weakly-supervised temporal action localization, in: *AAAI*, 2020, pp. 11320–11327.

- [13] S. Narayan, H. Cholakkal, F. S. Khan, L. Shao, 3c-net: Category count and center loss for weakly-supervised action localization, in: ICCV, 2019, pp. 8679–8687.
- [14] F. Ma, L. Zhu, Y. Yang, S. Zha, G. Kundu, M. Feiszli, Z. Shou, Sf-net: Single-frame supervision for temporal action localization, in: A. Vedaldi, H. Bischof, T. Brox, J. Frahm (Eds.), ECCV, Vol. 12349 of Lecture Notes in Computer Science, Springer, 2020, pp. 420–437.
- [15] P. Lee, H. Byun, Learning action completeness from points for weakly-supervised temporal action localization, in: ICCV, IEEE, 2021, pp. 13628–13637.
- [16] Z. Xia, J. Cheng, S. Liul, Y. Hu, S. Wang, Y. Zhang, L. Dang, Realigning confidence with temporal saliency information for point-level weakly-supervised temporal action localization, in: CVPR, IEEE, 2024, pp. 18440–18450.
- [17] M. Liu, L. Wang, S. Zhou, K. Xia, Q. Wu, Q. Zhang, G. Hua, Stepwise multi-grained boundary detector for point-supervised temporal action localization, in: A. Leonardis, E. Ricci, S. Roth, O. Russakovsky, T. Sattler, G. Varol (Eds.), ECCV, Vol. 15065 of Lecture Notes in Computer Science, Springer, 2024, pp. 333–349.
- [18] H. Zhang, X. Wang, X. Xu, Z. Qing, C. Gao, N. Sang, Hr-pro: Point-supervised temporal action localization via hierarchical reliability propagation, in: M. J. Wooldridge, J. G. Dy, S. Natarajan (Eds.), AAAI, AAAI Press, 2024, pp. 7115–7123.
- [19] J. Redmon, S. K. Divvala, R. B. Girshick, A. Farhadi, You only look once: Unified, real-time object detection, in: CVPR, IEEE Computer Society, 2016, pp. 779–788.
- [20] S. Ren, K. He, R. B. Girshick, J. Sun, Faster R-CNN: towards real-time object detection with region proposal networks, TPAMI 39 (6) (2017) 1137–1149.
- [21] A. Fathi, X. Ren, J. M. Rehg, Learning to recognize objects in egocentric activities, in: CVPR, IEEE Computer Society, 2011, pp. 3281–3288.

- [22] T. Lin, X. Zhao, H. Su, C. Wang, M. Yang, Bsn: Boundary sensitive network for temporal action proposal generation, in: ECCV, 2018, pp. 3–19.
- [23] T. Lin, X. Liu, X. Li, E. Ding, S. Wen, Bmn: Boundary-matching network for temporal action proposal generation, in: ICCV, 2019, pp. 3889–3898.
- [24] H. Ren, W. Yang, T. Zhang, Y. Zhang, Proposal-based multiple instance learning for weakly-supervised temporal action localization, in: CVPR, IEEE, 2023, pp. 2394–2404.
- [25] J. Li, T. Yang, W. Ji, J. Wang, L. Cheng, Exploring denoised cross-video contrast for weakly-supervised temporal action localization, in: CVPR, IEEE, 2022, pp. 19882–19892.
- [26] Y. Zhai, L. Wang, W. Tang, Q. Zhang, J. Yuan, G. Hua, Two-stream consensus network for weakly-supervised temporal action localization, in: A. Vedaldi, H. Bischof, T. Brox, J. Frahm (Eds.), ECCV, Vol. 12351 of Lecture Notes in Computer Science, Springer, 2020, pp. 37–54.
- [27] Y. Tewel, Y. Shalev, I. Schwartz, L. Wolf, Zerocap: Zero-shot image-to-text generation for visual-semantic arithmetic, in: IEEE/CVF Conference on Computer Vision and Pattern Recognition, CVPR 2022, New Orleans, LA, USA, June 18–24, 2022, IEEE, 2022, pp. 17897–17907.
- [28] Y. Su, T. Lan, Y. Liu, F. Liu, D. Yogatama, Y. Wang, L. Kong, N. Collier, Language models can see: Plugging visual controls in text generation, CoRR abs/2205.02655 (2022).
- [29] W. Li, L. Zhu, L. Wen, Y. Yang, Decap: Decoding CLIP latents for zero-shot captioning via text-only training, in: ICLR, OpenReview.net, 2023.
- [30] A. Radford, J. W. Kim, C. Hallacy, A. Ramesh, G. Goh, S. Agarwal, G. Sastry, A. Askell, P. Mishkin, J. Clark, G. Krueger, I. Sutskever, Learning transferable visual models from natural language supervision, in: ICML, 2021, pp. 8748–8763.

[31] A. Radford, J. Wu, R. Child, D. Luan, D. Amodei, I. Sutskever, et al., Language models are unsupervised multitask learners, *OpenAI blog* 1 (8) (2019) 9.

[32] J. Li, D. Li, S. Savarese, S. C. H. Hoi, BLIP-2: bootstrapping language-image pre-training with frozen image encoders and large language models, in: A. Krause, E. Brunskill, K. Cho, B. Engelhardt, S. Sabato, J. Scarlett (Eds.), *ICML*, Vol. 202 of *Proceedings of Machine Learning Research*, PMLR, 2023, pp. 19730–19742.

[33] H. Liu, C. Li, Q. Wu, Y. J. Lee, Visual instruction tuning, in: A. Oh, T. Naumann, A. Globerson, K. Saenko, M. Hardt, S. Levine (Eds.), *NeurIPS*, 2023.

[34] J. Alayrac, J. Donahue, P. Luc, A. Miech, I. Barr, Y. Hasson, K. Lenc, A. Mensch, K. Millican, M. Reynolds, R. Ring, E. Rutherford, S. Cabi, T. Han, Z. Gong, S. Samangooei, M. Monteiro, J. L. Menick, S. Borgeaud, A. Brock, A. Nematzadeh, S. Sharifzadeh, M. Binkowski, R. Barreira, O. Vinyals, A. Zisserman, K. Simonyan, Flamingo: a visual language model for few-shot learning, in: S. Koyejo, S. Mohamed, A. Agarwal, D. Belgrave, K. Cho, A. Oh (Eds.), *NeurIPS*, 2022.

[35] J. Carreira, A. Zisserman, Quo vadis, action recognition? A new model and the kinetics dataset, in: *CVPR*, IEEE Computer Society, 2017, pp. 4724–4733.

[36] B. Ni, H. Peng, M. Chen, S. Zhang, G. Meng, J. Fu, S. Xiang, H. Ling, Expanding language-image pretrained models for general video recognition, in: S. Avidan, G. J. Brostow, M. Cissé, G. M. Farinella, T. Hassner (Eds.), *ECCV*, Vol. 13664 of *Lecture Notes in Computer Science*, Springer, 2022, pp. 1–18.

[37] Z. Li, Y. Chai, T. Y. Zhuo, L. Qu, G. Haffari, F. Li, D. Ji, Q. H. Tran, FACTUAL: A benchmark for faithful and consistent textual scene graph parsing, in: A. Rogers, J. L. Boyd-Graber, N. Okazaki (Eds.), *ACL*, Association for Computational Linguistics, 2023, pp. 6377–6390.

[38] M. Minderer, A. A. Gritsenko, N. Houlsby, Scaling open-vocabulary object detection, in: A. Oh, T. Naumann, A. Globerson, K. Saenko, M. Hardt, S. Levine (Eds.), *NeurIPS*, 2023.

- [39] N. Bodla, B. Singh, R. Chellappa, L. S. Davis, Soft-nms - improving object detection with one line of code, in: ICCV, IEEE Computer Society, 2017, pp. 5562–5570.
- [40] R. Zeng, W. Huang, C. Gan, M. Tan, Y. Rong, P. Zhao, J. Huang, Graph convolutional networks for temporal action localization, in: ICCV, IEEE, 2019, pp. 7093–7102.
- [41] Z. Qing, H. Su, W. Gan, D. Wang, W. Wu, X. Wang, Y. Qiao, J. Yan, C. Gao, N. Sang, Temporal context aggregation network for temporal action proposal refinement, in: CVPR, Computer Vision Foundation / IEEE, 2021, pp. 485–494.
- [42] D. Sridhar, N. Quader, S. Muralidharan, Y. Li, P. Dai, J. Lu, Class semantics-based attention for action detection, in: ICCV, IEEE, 2021, pp. 13719–13728.
- [43] R. Zeng, W. Huang, M. Tan, Y. Rong, P. Zhao, J. Huang, C. Gan, Graph convolutional module for temporal action localization in videos, TPAMI 44 (10) (2022) 6209–6223.
- [44] C. Zhao, A. K. Thabet, B. Ghanem, Video self-stitching graph network for temporal action localization, in: ICCV, IEEE, 2021, pp. 13638–13647.
- [45] C. Lin, C. Xu, D. Luo, Y. Wang, Y. Tai, C. Wang, J. Li, F. Huang, Y. Fu, Learning salient boundary feature for anchor-free temporal action localization, in: CVPR, Computer Vision Foundation / IEEE, 2021, pp. 3320–3329.
- [46] Z. Yang, J. Qin, D. Huang, Acgnet: Action complement graph network for weakly-supervised temporal action localization, in: AAAI, AAAI Press, 2022, pp. 3090–3098.
- [47] L. Huang, L. Wang, H. Li, Weakly supervised temporal action localization via representative snippet knowledge propagation, in: CVPR, IEEE, 2022, pp. 3262–3271.
- [48] M. Chen, J. Gao, C. Xu, Uncertainty-aware dual-evidential learning for weakly-supervised temporal action localization, TPAMI 45 (12) (2023) 15896–15911.

[49] J. Zhou, L. Huang, L. Wang, S. Liu, H. Li, Improving weakly supervised temporal action localization by bridging train-test gap in pseudo labels, in: CVPR, IEEE, 2023, pp. 23003–23012.

[50] M. N. Rizve, G. Mittal, Y. Yu, M. Hall, S. Sajeev, M. Shah, M. Chen, Pivotal: Prior-driven supervision for weakly-supervised temporal action localization, in: CVPR, IEEE, 2023, pp. 22992–23002.

[51] W. Yun, M. Qi, C. Wang, H. Ma, Weakly-supervised temporal action localization by inferring salient snippet-feature, in: M. J. Wooldridge, J. G. Dy, S. Natarajan (Eds.), AAAI, AAAI Press, 2024, pp. 6908–6916.

[52] G. Lim, H. Kim, J. Kim, Y. Choi, Probabilistic vision-language representation for weakly supervised temporal action localization, in: J. Cai, M. S. Kankanhalli, B. Prabhakaran, S. Boll, R. Subramanian, L. Zheng, V. K. Singh, P. César, L. Xie, D. Xu (Eds.), ACM MM, ACM, 2024, pp. 5507–5516.

[53] D. Moltisanti, S. Fidler, D. Damen, Action recognition from single timestamp supervision in untrimmed videos, in: CVPR, Computer Vision Foundation / IEEE, 2019.

[54] L. Yang, J. Han, T. Zhao, T. Lin, D. Zhang, J. Chen, Background-click supervision for temporal action localization, TPAMI 44 (12) (2022) 9814–9829.

[55] J. Fu, J. Gao, C. Xu, Compact representation and reliable classification learning for point-level weakly-supervised action localization, TIP 31 (2022) 7363–7377.

[56] G. Li, D. Cheng, N. Wang, J. Li, X. Gao, Neighbor-guided pseudo-label generation and refinement for single-frame supervised temporal action localization, TIP 33 (2024) 2419–2430.

[57] S. M. Yoshida, T. Shibata, M. Terao, T. Okatani, M. Sugiyama, Action-agnostic point-level supervision for temporal action detection, CoRR abs/2412.21205 (2025).

- [58] C. Ju, P. Zhao, S. Chen, Y. Zhang, Y. Wang, Q. Tian, Divide and conquer for single-frame temporal action localization, in: ICCV, IEEE, 2021, pp. 13435–13444.
- [59] H. Idrees, A. R. Zamir, Y. Jiang, A. Gorban, I. Laptev, R. Sukthankar, M. Shah, The THUMOS challenge on action recognition for videos "in the wild", Computer Vision and Image Understanding 155 (2017) 1–23.
- [60] D. Damen, T. Leelasawassuk, O. Haines, A. Calway, W. W. Mayol-Cuevas, You-do, i-learn: Discovering task relevant objects and their modes of interaction from multi-user egocentric video, in: M. F. Valstar, A. P. French, T. P. Pridmore (Eds.), BMVA, BMVA Press, 2014.
- [61] F. C. Heilbron, V. Escorcia, B. Ghanem, J. C. Niebles, Activitynet: A large-scale video benchmark for human activity understanding, in: CVPR, IEEE Computer Society, 2015, pp. 961–970.
- [62] C. Schuhmann, R. Beaumont, R. Vencu, C. Gordon, R. Wightman, M. Cherti, T. Coombes, A. Katta, C. Mullis, M. Wortsman, P. Schramowski, S. Kundurthy, K. Crowson, L. Schmidt, R. Kaczmarczyk, J. Jitsev, LAION-5B: an open large-scale dataset for training next generation image-text models, in: S. Koyejo, S. Mohamed, A. Agarwal, D. Belgrave, K. Cho, A. Oh (Eds.), NeurIPS 2022, 2022.
- [63] A. Li, M. Thotakuri, D. A. Ross, J. Carreira, A. Vostrikov, A. Zisserman, The ava-kinetics localized human actions video dataset, CoRR abs/2005.00214 (2020).
- [64] X. Li, J. Li, Aoe: Angle-optimized embeddings for semantic textual similarity, in: L. Ku, A. Martins, V. Srikumar (Eds.), ACL, Association for Computational Linguistics, 2024, pp. 1825–1839.
- [65] T.-Y. Lin, P. Goyal, R. Girshick, K. He, P. Dollár, Focal loss for dense object detection, in: ICCV, 2017, pp. 2980–2988.